Pattern selection at the onset of Rayleigh-Bénard convection in a horizontal shear flow

Morten Tveitereid
Agder College of Engineering, N-4890 Grimstad, Norway

Hanns Walter Müller
Laboratoire de Physique, Ecole Normale Supérieure de Lyon, 69364 Lyon, France
and Institut für Theoretische Physik, Universität des Saarlandes, D-66041 Saarbrücken, Germany
(Received 18 February 1994)

We examine the onset of Rayleigh-Bénard convection in a horizontal fluid layer with an imposed weak shear flow. Convection patterns in the form of traveling transverse rolls and stationary longitudinal rolls are considered. The investigation is performed in the framework of amplitude equations which allow for slow variations of the order parameter field both in the streamwise coordinate and in time. By invoking the concept of absolute and convective instability of the basic state, it is shown that a nontrivial selection of the most unstable mode takes place. The role of noise upon the selection process is investigated by considering the spatial growth exponents for both types of structures.

PACS number(s): 47.54.+r, 47.20.Bp, 47.27.Te, 47.60.+i

I. INTRODUCTION

Rayleigh-Bénard convection (RBC) describes several phenomena of geophysical and industrial interest [1–3], and has been studied extensively both theoretically and experimentally [4]. During recent years, RBC has also played an important role in studies of nonlinear pattern forming systems, because the system describes a richness of bifurcations, pattern stability problems, and transition routes to chaos [4–6]. The system has the advantage over many other nonequilibrium systems that theoretical and experimental results can be compared quantitatively, because the boundary conditions and stress parameters of the system can be accurately controlled in laboratory experiments.

The topic of this article is to investigate the linear onset of buoyancy driven convection in a weak horizontal shear flow uniformly heated from below. RBC combined with the stability problem of a laminar shear flow (Orr-Sommerfeld problem) leads to an interesting bifurcation behavior [7]. Depending on the width of the convection channel and the rate of the shear flow used in experiments, either traveling convection rolls with axes perpendicular to the flow (transverse rolls, TR's) or stationary rolls aligned parallel to the flow (longitudinal rolls, LR's) are observed [7–13]. The linear and nonlinear dynamics of TR's have been explained successfully by Müller *et al.* [14] using the concept of absolute and convective instability [15]. Most experimental works have dealt with one of the two patterns. Only recently, experimental investigations have demonstrated the coexistence of TR's and LR's, albeit in different parts of the channel, or more complicated time dependent behavior [16,12,13]. Theoretical investigations with two coupled amplitude equations for TR's and LR's [17,18] have been used to understand the competitive dynamics of the two structures.

The linear stability of buoyancy driven convection in a horizontal shear flow is well understood [19,11,20]. When the temperature difference across the layer is larger than a critical value, the conduction state becomes (convectively) unstable, and convection in the form of TR's or LR's is set up. For an idealized situation of a fluid layer without lateral boundaries, plane wave perturbations in the form of LR's turn out to be unaffected by the flow while TR disturbances are stabilized. A convective pattern in the form of LR's is thus predicted to appear at a lower thermal forcing than the TR pattern. However, the present article shows that the *absolute* stability boundaries must be considered, and from this a natural pattern selection results favoring TR's if the flow is sufficiently weak. In previous publications [11,20] the experimental observation of TR's has been motivated by the additional stabilization due to lateral boundaries, which becomes remarkable only in narrow channels.

In the present paper we examine in detail the preferred pattern at the onset of convection. Nonlinear processes are not discussed. The starting point for the analysis is the linearized amplitude equations, which have been derived recently [18]. The absolute and convective instabilities of the basic conductive state are investigated, and the corresponding implications for the pattern selection are discussed. We put special emphasis on the question of which pattern may be detected in an experiment when noise is present in the system.

II. THE SYSTEM AND THE MODEL EQUATIONS

We consider RBC in a horizontal fluid layer between two rigid perfectly heat conducting top and bottom boundaries. A constant pressure gradient in the lateral

direction drives a shear flow with strength expressed by the dimensionless Reynolds number $\mathrm{Re}= U_0 d/\nu$. Here U_0 is the flow velocity averaged over the layer thickness d, and ν is the kinematic viscosity of the fluid. The second dimensionless control parameter is the Rayleigh number $\mathrm{Ra}= \alpha g d^3 \Delta T/(\kappa\nu)$, which measures the thermal forcing of the system. Here ΔT is the temperature difference between the cooled top and the heated bottom plate of the channel, α is the coefficient of thermal expansion, g is the acceleration due to gravity, and κ is the thermal diffusivity. We restrict the analysis to weak shear flows, i.e., small values of Re, and to Rayleigh numbers close above the threshold Ra_c. For $\mathrm{Ra}<\mathrm{Ra}_c$ there is no convection in the system. The basic conductive state is characterized by a plane Poiseuille flow and a temperature profile increasing linearly from the top to the bottom. When Ra is slightly larger than Ra_c, a convective cellular motion is set up and superimposes to the basic state. The governing equations for this physical system can be found in [18].

The linear stability problem of the basic state was first solved by Gage and Reid [19], who considered the case of a fluid layer without lateral sidewalls. They solved the linear stability problem by superimposing plane wave perturbations of the form

$$\phi(z)\, e^{i(Kx+Ly)+s(K,L,\mathrm{Re},\mathrm{Ra})t} \tag{2.1}$$

to the base flow. Here (x, y, z) denote the Cartesian coordinates with the x axis in the direction of the imposed flow and the z axis vertically upwards, t is the time, $\phi(z)$ is the eigenfunction satisfying the boundary conditions at the top and bottom plates, K and L are the respective wave numbers in x and y directions, and s is the complex temporal growth rate playing the role of the eigenvalue. It is found that Ra_c depends on Re and the direction of the lateral wave vector (K, L) [19]. Disturbances in the form of transverse rolls ($K \neq 0$, $L = 0$) are stabilized by the flow, and they start growing above the threshold $\mathrm{Ra}_c^T(\mathrm{Re})$ with wave number $K = K_c(\mathrm{Re})$. Here and in the following the sub- or superscripts T and L are referring to TR's and LR's, respectively. The stability threshold for rolls with any other wave vector is obtained from Ra_c^T by virtue of Squire's transformation [21,19], which gives

$$\mathrm{Ra}_c^{\varphi}(\mathrm{Re}) = \mathrm{Ra}_c^T(\mathrm{Re}\cos\varphi). \tag{2.2}$$

Here φ denotes the angle between the wave vector and the streamwise direction. In the case of LR's ($K = 0$, $L \neq 0$) the critical values become

$$\mathrm{Ra}_c^L = \mathrm{Ra}_c^T(\mathrm{Re}=0) = \mathrm{Ra}_{c0}\,, \quad L_c = K_c(\mathrm{Re}=0) = K_{c0}, \tag{2.3}$$

where $\mathrm{Ra}_{c0} = 1707.8$ and $K_{c0} = 3.116$ are the critical quantities without a shear flow. We now introduce the reduced Rayleigh number ε defined by

$$\varepsilon = (\mathrm{Ra} - \mathrm{Ra}_{c0})/\mathrm{Ra}_{c0}, \tag{2.4}$$

and let ε_c^T and ε_c^L denote the critical thresholds for TR's and LR's, respectively. Figure 1 displays how these critical thresholds depend on Re. At small flow rates ε_c^T increases quadratically in Re because the stabilization remains the same when the shear flow reverses direction. Since $\varepsilon_c^L(\mathrm{Re})=0$ in the absence of sidewalls, the two curves intersect at $\mathrm{Re}=\mathrm{Re}^* = 0$. As shown by the inset of Fig. 1, the stability behavior in a channel of *finite* width (i.e., in the presence of sidewalls) is qualitatively different and leads to a *finite* value of Re^*. This effect becomes remarkable in narrow channels [11,20].

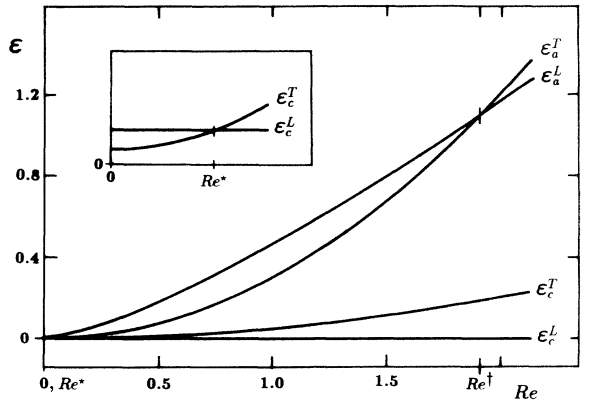

FIG. 1. Sketch of the linear stability boundaries for a channel without lateral sidewalls. The conductive state is convectively (absolutely) unstable with respect to traveling transverse rolls for $\varepsilon > \varepsilon_c^T$ (ε_a^T), and with respect to stationary longitudinal rolls for $\varepsilon > \varepsilon_c^L$ (ε_a^L). $\mathrm{Re}^*=0$ and Re^+ define the respective intersections between the convective and the absolute thesholds. Re^* becomes nonzero for a channel with lateral sidewalls, as shown in the inset figure.

From the above discussion, which is based on a plane wave stability analysis, one usually concludes [11,19,20] that the cellular pattern at the onset of convection is traveling TR's for $\mathrm{Re}<\mathrm{Re}^*$ but stationary LR's for $\mathrm{Re}>\mathrm{Re}^*$. However, this statement does not strictly apply, because in an experimental situation the convection channel is of *finite length*: Spatially extended perturbations like plane waves of the form $\exp(iKx)$ are thus unrealistic modes, and an investigation of disturbances which are localized in the streamwise direction is more appropriate. In this context the critical threshold $\varepsilon_c^{T,L}$ is also called the *convective* boundary. For values of ε close above it, localized perturbations are growing in a comoving frame of reference, but they decay in the laboratory frame. The perturbations are advected by the shear flow, and they can be swept out of the channel before their amplitudes exceed a detectable limit. Temporally growing amplitudes in the *lab frame* are only achievable if the thermal forcing ε is lifted above the higher *absolute* boundary $\varepsilon_a^{T,L}$.

In order to determine the absolute stability and to investigate the linear growth of small localized perturbations we do not rely on the basic hydrodynamic equations but perform the investigation in the framework of the amplitude equations. This is a powerful tool to describe the dynamics close above the convective threshold. For ε slightly greater than $\varepsilon_c^{T,L}$ the convective contributions to the order parameter fields are given by

$$A\phi_T(z)\, e^{i(K_c x-\Omega_c t)}, \quad B\phi_L(z)\, e^{iL_c y}, \tag{2.5}$$

TABLE I. The leading-order Re expansions of the coefficients of the envelope equations (2.6) for a channel of infinite lateral extent and rigid perfectly heat conducting top and bottom boundaries, and for a fluid of Prandtl number 5.8.

$\tau_T = 0.0554$	$v_T = 7.5070\mathrm{Re}$
$\tau_L = 0.0554$	$v_L = 7.4350\mathrm{Re}$
$\gamma_T = 0.1482$	$c_0 = 0.0187\mathrm{Re}$
$\gamma_L = 0.0010\mathrm{Re}^2$	$c_1 = 0.0382\mathrm{Re}$
$\lambda_L = 0.0038$	$\beta_L = 0.0002\mathrm{Re}$

where A and B represent the respective amplitudes of TR and LR perturbations. Patterns in the form of oblique rolls are not considered since they are not observed in experiments. The amplitudes A,B are supposed to vary slowly in time and in the horizontal directions x and y. However, for the sake of simplicity we neglect the y dependence and thus confine our analysis to LR patterns with a frozen wave vector $L = L_c$. A detuning from this value is not allowed. The evolution equations for A and B have been derived in a recent publication [18]. Here we only need the linearized versions and obtain

$$\tau_T(\partial_t + v_T\partial_x)A = (\varepsilon - \varepsilon_c^T)(1 + ic_0)A + \gamma_T(1 + ic_1)\partial_x^2 A\ , \quad (2.6a)$$

$$\tau_L(\partial_t + v_L\partial_x)B = (\varepsilon - \varepsilon_c^L)B + \gamma_L\partial_x^2 B + \beta_L\partial_x^3 B - \lambda_L\partial_x^4 B. \quad (2.6b)$$

Close above the convective onset these equations reflect the linear dynamics of TR and LR perturbations as governed by the basic hydrodynamic equations. Table I gives the leading-order Re expansion of the coefficients as calculated in [18] for a fluid with a Prandtl number of 5.8. The coefficients of Eq. (2.6b) are real, which follows from the stationary character of the LR instability and the reflection symmetry at the plane $y = 0$. Observe that v_T, v_L, β_L, and the imaginary parts c_0 and c_1 are odd functions of Re, while the other coefficients are even. This is a general result of the $x \to -x$ symmetry of the system under simultaneous reversal of the flow direction (Re $\to -$ Re). Equations (2.6) have been computed [18] for a fluid layer without sidewalls, where $\varepsilon_c^L = 0$. In the present paper we also restrict ourselves to this idealized situation. Our predictions will therefore asymptotically apply to experiments which are performed in convection channels with a large ratio of width to height, i.e., aspect ratio $\Gamma \gg 1$.

III. PATTERN SELECTION AT THE ONSET OF CONVECTION

A. Absolute and convective stability of the basic state

The homogeneous convectionless state of the system is characterized by the trivial solution of Eqs. (2.6):

$$A = B = 0\ . \quad (3.1)$$

As typically for open flow systems, this basic state becomes convectively unstable beyond a threshold ε_c, but absolutely unstable above a higher boundary ε_a [15]. This distinction is based on the different dynamical behavior of small localized perturbations: In the convectively unstable parameter region, $\varepsilon_c < \varepsilon < \varepsilon_a$, localized disturbances are growing in a comoving frame of reference, but they die out at any fixed location in the lab frame as they are advected by the flow. Localized perturbations start growing in the lab frame only for sufficiently strong driving. This defines the absolute boundary ε_a. We emphasize the importance of considering *localized perturbations* in open flow experiments because spatially extended disturbances, like the plane wave $\exp(iKx)$, are unrealistic modes in geometries which are limited in the streamwise direction (by an inlet and an outlet). Usually one determines the convective or critical threshold ε_c by a conventional plane wave stability analysis (with a *real* wave vector). One can also examine the temporal evolution of a localized perturbation in a frame of reference where the center of the disturbance is at rest [22]. The latter method, even though mathematically more intricate, has the advantage of giving both the convective and the absolute threshold by just regarding the evolution of the perturbations in two different frames. The present analysis requires a separate consideration of perturbations in the form of TR's and LR's.

The stability of the basic state with respect to TR's is governed by Eq. (2.6a). For an initial condition of the form $A(x, t = 0) = \delta(x)$ (Dirac's δ function) the problem is solved by exact integration, giving for $t > 0$

$$A(x,t) = \frac{(1 + ic_1)^{-1/2}}{\sqrt{4\gamma_T\pi t/\tau_T}} \exp\left\{ \frac{\varepsilon - \varepsilon_c^T}{\tau_T}(1 + ic_0)t - \frac{(x - v_T t)^2\tau_T}{4\gamma_T(1 + ic_1)t} \right\}. \quad (3.2)$$

The asymptotic time evolution for $t \to \infty$ is determined by the sign of the growth exponent G_T, which for any position x and time t reads

$$G_T = \frac{\varepsilon - \varepsilon_c^T}{\tau_T} - \frac{(x - v_T t)^2\tau_T}{4\gamma_T(1 + c_1^2)t^2}\ . \quad (3.3)$$

The maximum value of G_T appears in a frame of reference moving along the ray $x/t = v_T$. In this frame TR perturbations are growing if $\varepsilon > \varepsilon_c^T$, thus recovering the threshold of convective instability as obtained by the usual plane wave analysis. In order to obtain the absolute stability boundary we solve $G_T = 0$ in the lab frame, i.e., along the ray $x/t = 0$. Thereby we recover Deissler's [23–25] result $\varepsilon_a^T = \varepsilon_c^T + \Delta\varepsilon^T$, with

$$\Delta\epsilon^T = \frac{(\tau_T v_T)^2}{4\gamma_T(1 + c_1^2)}\ . \quad (3.4)$$

Figure 1 shows that for a weak flow ε_a^T depends quadratically on Re since v_T^2 does so.

To get the behavior of LR perturbations we pose the same initial-value problem for Eq. (2.6b). Since an exact integration is not possible, we treat this problem perturbatively for small flow rates Re, and we use the method of steepest descent [26] to obtain the asympotic solution for large values of t. Details of this calculation are relegated to the Appendix. In any frame of reference where x/t satisfies the condition $O(v_L - x/t) \leq O(v_L)$, the growth exponent for LR's turns out to be

$$G_L = \frac{\varepsilon - \varepsilon_c^L}{\tau_L} - \frac{3\lambda_L}{2\tau_L}\chi^{\frac{4}{3}}\left[1 + O(\mathrm{Re}^{\frac{2}{3}})\right], \tag{3.5}$$

where $\chi = (v_L t - x)\tau_L/(4\lambda_L t)$. The frame which moves with the center of the disturbance propagates along the ray $x/t = v_L$. Thus, for $\chi = 0$ we reobtain the convective threshold for LR perturbations at $\varepsilon = \varepsilon_c^L = 0$. Moreover, to find the absolute boundary we solve $G_L = 0$ in the lab frame $x/t = 0$ and get $\varepsilon_a^L = \varepsilon_c^L + \Delta\varepsilon^L$, where

$$\Delta\varepsilon^L = \frac{3\lambda_L}{2}\left(\frac{v_L\tau_L}{4\lambda_L}\right)^{\frac{4}{3}}\left[1 + O(\mathrm{Re}^{\frac{2}{3}})\right]. \tag{3.6}$$

The stability boundaries $\varepsilon_c^{T,L}$, $\varepsilon_a^{T,L}$ are depicted in Fig. 1. For small flow rates the absolute boundaries ε_a^T and ε_a^L, respectively, increase in the same way as Re^2 and $\mathrm{Re}^{4/3}$ increase. Thus we obtain an intersection point at some nonzero value of Re, which we identify as $\mathrm{Re}^\dagger$. Recall that the quantity $\mathrm{Re}^\star$ corresponds to the intersection of the two *convective* boundaries ε_c^T and ε_c^L. It is interesting to note that the intersection point $\mathrm{Re}^\dagger$, unlike $\mathrm{Re}^\star$, is finite in wide channels. Thus the present amplitude equation analysis predicts a natural pattern selection at the onset of convection by which TR perturbations are initiated before LR's for $\mathrm{Re}<\mathrm{Re}^\dagger$, while LR's are detected first if $\mathrm{Re}>\mathrm{Re}^\dagger$. This is opposite to earlier theories [19,11,20] where the transition from the TR to the LR onset has been associated with $\mathrm{Re}^\star$. By using this identification one has concluded from the relation $\mathrm{Re}^\star \to 0$ as $\Gamma \to \infty$ that no linear pattern selection takes place in wide channels: LR's are always more unstable than TR's throughout the whole Re axis [19]. Accordingly, the experimental observation of TR's could only be motivated in narrow channels ($\Gamma \sim 1$), where $\mathrm{Re}^\star$ is finite [11,20].

It is known that convectively unstable open flow systems react very sensitively upon external disturbances [23–25]. The inevitable presence of external perturbations in such experiments (inlet turbulence and/or thermal noise) will make a direct measurement of $\mathrm{Re}^\dagger$ impossible or at least very difficult. Therefore, in the next section we will examine the growth of disturbances which are caused by external noise.

B. The onset of noise-sustained convection

In the above discussion we relate the onset of TR or LR convection to the absolute stability boundaries $\varepsilon_a^{T,L}$. This statement strictly applies to (idealized) systems which are free of any persistent sources of perturbations. In the present section we investigate how the results of Sec. III A must be modified if the influence of a given amount of background noise is taken into account. From the works of Deissler [23–25] it is known that continuous sources of noise, in convectively unstable open flow systems, make convection appear even below the absolute stability boundary. This phenomenon of "noise-sustained convection" arises from a downstream amplification of disturbances originating farther upstream. Even though perturbations and especially thermal noise may be generated at any position within the channel, those disturbances originating from the inlet are amplified most since they have the largest distance to grow. Consequently, instead of treating a spatially extended noise source, we consider a point source located at the inlet. Mathematically this source can be realized by imposing the boundary conditions

$$A(x = 0, t) = B(x = 0, t) = N(t)\ . \tag{3.7}$$

For simplicity we consider a complex white noise $\langle N(t)N^\star(t')\rangle = N_0^2\delta(t - t')$ of zero mean $\langle N(t)\rangle = 0$. At some downstream position x_0, which depends on the control parameters ε and Re, the noise is sufficiently amplified for the convective amplitude to exceed a defined threshold of detection D_0 [e.g., take $D_0 = 0.1\times$ (saturation amplitude), or identify D_0 with the resolution of the detector]. The spatial amplification of noise between the inlet and x_0 is governed by Eqs. (2.6) and obeys an exponential law of the form $\exp(\kappa x)$. Corresponding measurements have been performed by Babcock *et al.* [26,27] and Tsameret and Steinberg [28] on the Taylor-Couette system to detect the onset of noise-sustained Taylor vortex flow. In RBC onset experiments have been performed by Hwang and Liu [29] and Chiu and Rosenberger [9]. They investigate an isothermal fluid (kept at the temperature of the upper plate) entering the differentially heated test section of the channel. Thus, depending on the flow rate Re, the temperature field needs a certain entrance length before it adopts the linear profile and buoyancy driven convection may set in. This setup does not directly compare with our model, because our approach assumes a fluid being perfectly equilibrated to the basic convection-less state before entering into the channel. The stability problem related to the experiments in [29,9] has been investigated by Hwang and Cheng [30]. However, their result gives no satisfactory quantitative explanation of the measurements. The reason may be due to the fact that they ignored the influence of perturbations and did not discriminate between the absolute and convective nature of the instability.

We continue by considering the inlet-noise signal as a superposition of Fourier modes of the form $\exp(i\omega t)$. To each mode we relate a coefficient with the x dependency $\exp(\kappa x)$. Here $\kappa = \kappa(\omega, \varepsilon, \mathrm{Re})$ is the complex spatial growth exponent with real and imaginary parts to be denoted by a prime and a double prime, respectively. The characteristic polynomials for κ_T and κ_L are obtained from Eqs. (2.6) by taking the Fourier transform in t. We determine the value of ω for which the spatial growth rate κ' is a maximum by imposing $\partial\kappa'/\partial\omega = 0$. After some algebra we find that the TR mode with the largest growth in the downstream direction is characterized by

$$\tau_T v_T \tilde{\kappa}'_T = (\varepsilon - \varepsilon_c^T) + \gamma_T (1 + c_1^2)\tilde{\kappa}'^2_T \ , \tag{3.8a}$$

$$\tilde{\kappa}''_T = -c_1 \tilde{\kappa}'_T \ , \tag{3.8b}$$

$$\tau_T \tilde{\omega}_T = (c_0 + c_1)(\varepsilon - \varepsilon_c^T) \ . \tag{3.8c}$$

Here the tilde indicates values after the maximization with respect to ω. The corresponding characteristic values for LR's are

$$\tau_L v_L \tilde{\kappa}'_L = \varepsilon + 8\lambda_L \tilde{\kappa}'^4_L + O(\mathrm{Re}^2), \tag{3.9a}$$

$$\tilde{\kappa}''_L = \pm\sqrt{3}\tilde{\kappa}'_L + O(\mathrm{Re}), \tag{3.9b}$$

$$\tau_L \tilde{\omega}_L = \mp\sqrt{3}\varepsilon + O(\mathrm{Re}^2), \tag{3.9c}$$

which are obtained by using $\varepsilon_c^L = 0$ and expanding $\tilde{\kappa}_L$ in powers of small Re with the leading term of $O(\mathrm{Re}^{\frac{1}{3}})$. Note that the coefficients γ_L and β_L [which are small of $O(\mathrm{Re}^2)$ and $O(\mathrm{Re})$, respectively] do not enter, meaning that the second and third space derivative terms of Eq. (2.6b) give no contribution, if the throughflow is sufficiently weak. Equations (3.8a) and (3.9a) implicitly define the maximum spatial growth rates $\tilde{\kappa}'_{T,L}(\varepsilon, \mathrm{Re})$. In order to describe the downstream growth of small perturbations, we have chosen the eigenvalue branch which gives zero growth at the convective boundary. This choice guarantees that all Fourier modes are damped in the parameter region where the basic convectionless state is stable. For slightly supercritical drive, $\varepsilon_c^{T,L} < \varepsilon < \varepsilon_a^{T,L}$, the real part of $\tilde{\kappa}_{T,L}$ becomes positive resulting in a narrow frequency band around $\tilde{\omega}_{T,L}$ which is spatially amplified. This is the principle of selective amplification, recently discussed by Deissler [24,25]. Mathematically this phenomenon manifests in a space-dependent noise spectrum governed by

$$S_{T,L}(x, \omega, \varepsilon, \mathrm{Re}) = N_0^2 \exp\{2\kappa'_{T,L}(\omega, \varepsilon, \mathrm{Re})x\}. \tag{3.10}$$

Here $S_{T,L}$ is the temporal Fourier transformation of the autocorrelation functions $\langle A(x,t)A^*(x,t+\Delta t)\rangle$ and $\langle B(x,t)B^*(x,t+\Delta t)\rangle$, respectively. Far enough downstream the white inlet noise $S_{T,L}(x=0,\omega,\varepsilon,\mathrm{Re}) = N_0^2$ is transformed into a narrow band spectrum which is sharply peaked around the frequency $\tilde{\omega}_{T,L}(\varepsilon, \mathrm{Re})$, where $\kappa'_{T,L}$ is maximum.

In Fig. 2 we present the ε-Re control parameter plane with lines of constant values of the spatial growth rates $\tilde{\kappa}'_{T,L}$, as defined by Eqs. (3.8a) and (3.9a). It turns out that each isoline intersects the respective absolute boundary line $\varepsilon_a^{T,L}$ only once, and that the two lines have the same slope at the point of intersection. To interpret the isolines physically we can imagine an experiment in which a detector (e.g., a laser Doppler velocimeter) is located at a downstream position x_0. Then, keeping the flow rate fixed, we carefully increase ε in order to increase the growth rates $\kappa'_{T,L}$. Depending on whether $\tilde{\kappa}'_T$ or $\tilde{\kappa}'_L$ first exceeds the threshold $(1/x_0)\ln(D_0/N_0)$, we detect the onset of either TR's or LR's. As an example, let us assume $(1/x_0)\ln(D_0/N_0) = 0.3$. Then we obtain from Fig. 2 that the isolines $\tilde{\kappa}'_T = \tilde{\kappa}'_L = 0.3$ intersect at $\mathrm{Re}^{\otimes} \simeq 1.15$. Below this flow rate the first pattern to occur at onset is TR, while it is LR for Re>$\mathrm{Re}^{\otimes}$. It would be interesting to test this prediction by a real experiment. We expect the best quantitative agreement when the measurements are taken in wide convection cells, where Eqs. (2.6) and their coefficients apply best.

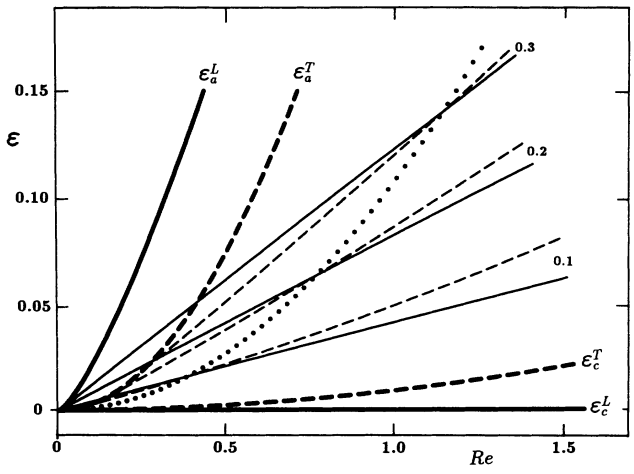

FIG. 2. Thin lines represent paths of constant spatial amplification in the ε-Re control parameter plane, i.e., $\tilde{\kappa}'_T$, $\tilde{\kappa}'_L$ = const (as indicated in the plot) for TR's (solid) and LR's (dashed). The dotted line joins all points where corresponding isolines for TR's and LR's intersect. Thus $\tilde{\kappa}'_T > \tilde{\kappa}'_L$ below this line, and vice versa above. The absolute and convective stability boundaries are displayed by thick lines.

Note that the transition point $\mathrm{Re}^{\otimes}$ is not uniquely related to a certain inlet-noise level N_0. This is because $\mathrm{Re}^{\otimes}$ is a function of the parameter combination $(1/x_0)\ln(D_0/N_0)$, i.e., the position of the detector x_0 and the onset amplitude D_0 are also entering the result. Using $\lambda_L \tilde{\kappa}'^3_L \ll \tau_L v_L$ and $\tau_T v_T \simeq \tau_L v_L$ for small Re, it follows from Eqs. (3.8a) and (3.9a) that

$$(1/x_0)\ln(D_0/N_0) \simeq \sqrt{\varepsilon_c^T/\gamma_T} \ . \tag{3.11}$$

This approximation is displayed in Fig. 3 (dashed), together with the exact numerical solution (solid). Note that the value of $\mathrm{Re}^{\otimes}$ increases linearly with $(1/x_0)\ln(D_0/N_0)$ for small Re. Knowing the experimental parameters D_0 and x_0 the measurement of $\mathrm{Re}^{\otimes}$ might give a useful means to estimate the inlet-noise strength N_0.

We now turn to the interpretation of $\tilde{\kappa}''_{T,L}$ and $\tilde{\omega}_{T,L}$. The finite imaginary part $\tilde{\kappa}''_T$ and frequency $\tilde{\omega}_T$ correct the wave number and frequency of the TR pattern. The TR mode with the largest spatial amplification therefore exhibits a wave number $K = (K_c + \tilde{\kappa}''_T)$ and a frequency $\Omega = (-\Omega_c + \tilde{\omega}_T)$. Moreover, Eqs. (3.9) define a pair of complex conjugate solutions, so that the LR envelope takes the form $B(x,t) \propto \exp(\tilde{\kappa}'_L x)\cos(\tilde{\kappa}''_L x + \tilde{\omega}_L t)$. Multiplication with the critical space dependence of LR's

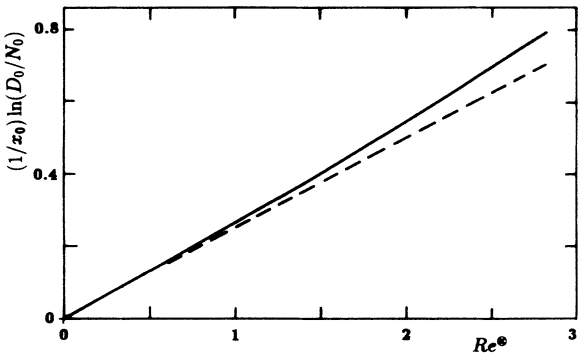

FIG. 3. The transition flow rate $\mathrm{Re}^{\otimes}$, at which the preferred noise-sustained pattern at onset switches between TR and LR, is a function of the inlet-noise level N_0, the position of the detector x_0, and the definition of the onset amplitude D_0. This relation is approximately given by Eq. (3.11) (dashed). The solid line is generated numerically from Eqs. (3.8a) and (3.9a).

$\exp(iL_c y)$, results in a LR pattern whose amplitude is slowly modulated by a downstream traveling wave. We mention that time dependent LR patterns have been observed in earlier experiments [9], but they are associated either with a superimposed TR pattern or with contributions from upstream turbulence. To our knowledge the possibility of modulated LR's has not yet been considered in the literature. In order to decide this question experimentally local techniques like laser Doppler velocimetry or hot-wire anemometry are inappropriate. Rather one needs a global pattern visualization as provided, for instance, by the shadowgraph method.

IV. SUMMARY AND DISCUSSION

In the present paper we investigate the stability of Rayleigh-Bénard convection subject to a horizontal shear flow. Absolute and convective stability boundaries are determined for the two kinds of competing perturbations: traveling transverse (TR's) and stationary longitudinal rolls (LR's). The analysis is based on the corresponding amplitude equations, which have been derived earlier. Spatially extended plane wave perturbations become unstable for values of the Rayleigh number above the *convective* boundaries $\varepsilon_c^{T,L}$. Since $\varepsilon_c^L \leq \varepsilon_c^T(\mathrm{Re})$ in convection channels with large width to height ratios, one usually has concluded that the preferred pattern at onset of instability is LR's. However, in the present paper we argue that, instead of considering plane waves, localized perturbations must be regarded which become unstable above the higher *absolute* boundaries $\varepsilon_a^{T,L}(\mathrm{Re})$. Knowing ε_a^T from earlier work we determine the threshold ε_a^L by an expansion in the flow rate Re. We observe an intersection between ε_a^T and ε_a^L at a finite flow rate $\mathrm{Re}^{\dagger}$. For flow rates below (above) $\mathrm{Re}^{\dagger}$ the analysis predicts TR's (LR's) to appear first at the onset of convection. This, however, is an idealized result, being valid only in the absence of perturbations. We therefore examine how these results are modified in the presence of a persistent noise source. Quantitative predictions about the observability of either of the two patterns at the onset of convection are given.

We emphasize that the results of the present paper are obtained on the basis of *linearized* amplitude equations. Therefore, our predictions apply to regions where the amplitude of convection is small compared to the saturation value. Conclusions about the prevailing pattern far downstream or about nonlinear selection and instability mechanisms cannot be drawn.

Another limitation of the model arises from the restriction to purely t- and x-dependent amplitude equations. By ignoring the slow horizontal space dependencies transverse to the flow (y dependence) the periodicity of LR's is fixed at the critical wave vector $L = L_c$. Calculations with the x- and y-dependent amplitude equations indicate that the most unstable wavelength of LR's is larger than the critical value L_c. However, farther downstream in the saturated convective region this selective effect will probably be covered by other instability mechanisms (Eckhaus, zigzag, or cross roll), which delimit the band of allowed wave numbers. These instability mechanisms, even though well understood in the classical Rayleigh-Bénard system, are shifted in the presence of the flow because the absolute and convective nature of these instabilities must be taken into account. We will treat these issues in a succeeding publication.

ACKNOWLEDGMENTS

Support by the Deutsche Forschungsgemeinschaft and the EEC is gratefully acknowledged.

APPENDIX: THE ABSOLUTE STABILITY BOUNDARY FOR LR'S

Here we solve the initial-value problem:

$$(\partial_T + V\partial_x)B = \nu B + \gamma\partial_x^2 B + \beta\partial_x^3 B - \partial_x^4 B\ , \qquad \text{(A1a)}$$

$$B(x,T) \to 0\ ,\ \text{as}\ |x| \to \infty \quad \text{and} \quad B(x,0) = \delta(x)\ , \qquad \text{(A1b)}$$

where $\delta(x)$ is the Dirac δ function. Equation (A1a) follows from Eq. (2.6b) if

$$T = \frac{\lambda_L}{\tau_L}t, \quad V = \frac{v_L\tau_L}{\lambda_L}, \quad \nu = \frac{\varepsilon - \varepsilon_c^L}{\lambda_L}, \qquad \text{(A2)}$$

$$\gamma = \frac{\gamma_L}{\lambda_L}\ , \quad \beta = \frac{\beta_L}{\lambda_L}\ .$$

We solve this initial-value problem by the method of Laplace and Fourier transforms, respectively defined by

$$\bar{f}(x,s) = \int_0^\infty e^{-sT} f(x,T)dT,$$

$$\tilde{f}(k,T) = \int_{-\infty}^{\infty} e^{-ikx} f(x,T)dx.$$

The corresponding inverse transforms are

$$f(x,T) = \frac{1}{2\pi i}\int_{s_0-i\infty}^{s_0+i\infty} e^{sT}\bar{f}(x,s)ds,$$

$$f(x,T) = \frac{1}{2\pi}\int_{-\infty}^{\infty} e^{ikx}\tilde{f}(k,T)dk,$$

where s_0 is real, and the contour $s = s_0$ lies to the right of all singular points of $\bar{f}(x,s)$ in the complex s plane.

By taking the Laplace and Fourier transforms of (A1) we find

$$\bar{\tilde{B}}(k,s) = (s - \nu + ikV + k^2\gamma + ik^3\beta + k^4)^{-1}\ , \quad \text{(A3)}$$

which has a simple pole in s. By using the residue theorem, the inverse Laplace transform gives

$$\tilde{B}(k,T) = \exp\{(\nu - ikV - k^2\gamma - ik^3\beta - k^4)T\}\ . \quad \text{(A4)}$$

Furthermore, applying the inverse Fourier transform to $\tilde{B}(k,T)$ yields

$$B(x,T) = \frac{1}{2\pi}e^{\nu T}\int_{-\infty}^{\infty} e^{-\psi T}dk, \quad \text{(A5a)}$$

where

$$\psi = k^4 + ik^3\beta + k^2\gamma + ik\left(V - \frac{x}{T}\right). \quad \text{(A5b)}$$

In the following we determine asymptotic expressions of the inverse Fourier transform for large values of T.

First we consider the case where $(V - x/T)$ is very small, i.e., in a frame of reference moving along the ray $x/T = V$. When $T \to \infty$ (or better for large values of $\gamma^2 T$), it follows immediately that

$$B(x,T) \sim \frac{1}{\sqrt{\gamma\pi T}}e^{\nu T}. \quad \text{(A6)}$$

Next, when $(V - x/T)$ is nonvanishing, we determine the integral perturbatively by expanding ψ in powers of small values of Re, and using the method of steepest descents [26]. Below we demonstrate the case where $O(V - x/T) = O(V) = O(\mathrm{Re})$, which is the actual situation in a lab frame as $T \to \infty$. To calculate the saddle points we consider the expansions:

$$\left(V - \frac{x}{T}\right) = \mathrm{Re}\left[4a_0^3 + O(\mathrm{Re}^2)\right], \quad \text{(A7a)}$$

$$\gamma = \mathrm{Re}^2\left[\gamma_0 + O(\mathrm{Re}^2)\right], \quad \text{(A7b)}$$

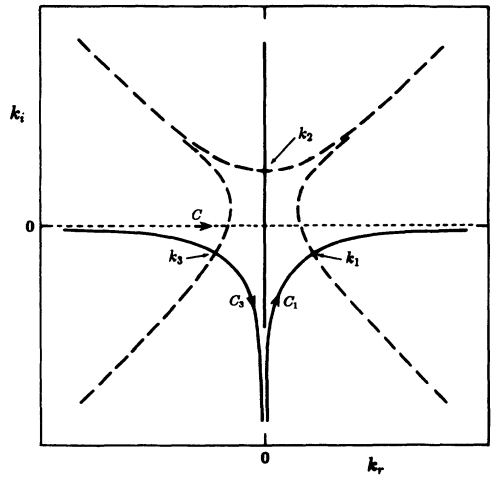

FIG. 4. The saddle points k_n $(n = 1,2,3)$, the steepest-descent curves (solid), and the steepest-ascent curves (dashed) of the function $-\psi$ (Eq. A5b) in the complex k plane. The original integration contour C (along the real axis) of (A5a) is deformed into the contour $C_3 + C_1$.

$$\beta = \mathrm{Re}\left[\beta_0 + O(\mathrm{Re}^2)\right], \quad \text{(A7c)}$$

where now (x/T) has been included in the leading term, and a_0 is positive. Thus the values of k at the saddle points, given by $\partial\psi/\partial k = 0$, can be written

$$k_n = \mathrm{Re}^{\frac{1}{3}}\left[k_{n0} + \mathrm{Re}^{\frac{2}{3}}k_{n1} + \mathrm{Re}^{\frac{4}{3}}k_{n2} + O(\mathrm{Re}^2)\right],$$

$$n = 1,2,3, \quad \text{(A8a)}$$

where

$$k_{n0} = a_0 e^{i(4n-5)\frac{\pi}{6}}, \quad k_{n1} = -\frac{i}{4}\beta_0,$$

$$k_{n2} = -\frac{1}{6k_{n0}}(\gamma_0 + \tfrac{3}{8}\beta_0^2). \quad \text{(A8b)}$$

Figure 4 displays the saddle points k_n, and the steepest curves of $-\psi$ which are defined by $\mathrm{Im}[\psi - \psi(k_n)] = 0$. There are two steepest-descent curves (the solid lines C_n) and two steepest-ascent curves (broken lines) emerging from each saddle point. To solve the integral in Eq. (A5a) we deform the original contour of integration, which runs from $-\infty$ to ∞ along the real k axis, to the contour $C_3 + C_1$. Taylor-series expansion of ψ about $k = k_n$, and evaluating the integral along the steepest-descent curve C_n, gives

$$\int_{C_n} e^{-\psi T}dk = e^{-\psi(k_n)T}\int_{C_n} e^{-\frac{1}{2}\psi''(k_n)(k-k_n)^2 T + \cdots}dk$$

$$= e^{-\psi(k_n)T}\sqrt{\frac{2\pi}{|\psi''(k_n)|\,T}}\,e^{i\vartheta_n}\left[1 + O\left(\frac{1}{T}\right)\right] \quad \text{as } T \to \infty, \quad \text{(A9)}$$

where the double prime denotes the twofold derivative with respect to k. Furthermore,

$$\psi(k_n) = \mathrm{Re}^{\frac{4}{3}}[3ik_{n0} + \mathrm{Re}^{\frac{2}{3}}\beta_0 - i\mathrm{Re}^{\frac{4}{3}}(\gamma_0 + \tfrac{3}{8}\beta_0^2)/k_{n0} + O(\mathrm{Re}^2)]a_0^3, \quad \text{(A10a)}$$

$$\psi''(k_n) = \mathrm{Re}^{\frac{2}{3}}\left[k_{n0} + \mathrm{Re}^{\frac{4}{3}}k_{n2} + O(\mathrm{Re}^2)\right] 12k_{n0}, \quad \text{(A10b)}$$

$$\vartheta_n = -\tfrac{1}{2}\arg[\psi''(k_n)]. \quad \text{(A10c)}$$

Finally, by using this result for the contour integration along C_3+C_1, the asymptotic solution of the initial-value problem (A1) becomes

$$B(x,T) = \sqrt{\frac{2}{|\psi''(k_1)|\,\pi T}}\, e^{(\nu-\psi_r)T}\cos(\psi_i T - \vartheta_1) \times \left[1 + O\left(\frac{1}{T}\right)\right] \quad \text{as } T \to \infty, \quad \text{(A11)}$$

where ψ_r and ψ_i denote the real and imaginary parts of $\psi(k_1)$, respectively. We notice that ψ_r is positive, giving that the most unstable perturbation is moving along the ray $x/T = V$ [see Eq. (A6)].

[1] E. Palm and M. Tveitereid, Norsk Geogr. Tidsskr. **31**, 145 (1977).

[2] A. Ludvigsen and E. Palm, J. Geophys. Res. **97**, 12 315 (1992).

[3] C. Dietsche and U. Müller, J. Fluid Mech. **161**, 249 (1985).

[4] P. Manneville, in *Dissipative Structures and Weak Turbulence*, edited by H. Araki, A. Libchaber, and G. Parisi (Academic, San Diego, 1990), p. 95, and references cited therein.

[5] H. L. Swinney and J. P. Gollub, *Hydrodynamic Instabilities and the Transition to Turbulence*, 2nd ed. (Springer, Berlin, 1985).

[6] M. Tveitereid, E. Palm, and A. Skogvang, Dyn. Stability Syst. **1**, 343 (1986).

[7] For a review, see R. E. Kelly, in *Proceedings of the International Conference on Physical Chemistry and Hydrodynamics*, edited by D. B. Spalding (Advance Publ., London, 1977), p. 65.

[8] J. M. Luijkx and J. K. Platten, Int. J. Heat Mass Transfer **24**, 1287 (1981).

[9] K. C. Chiu and F. Rosenberger, Int. J. Heat Mass Transfer **30**, 1645 (1987).

[10] A. Pocheau, V. Croquette, P. Le Gal, and C. Poitou, Europhys. Lett. **3**, 915 (1987).

[11] J. M. Luijkx, Ph.D. thesis, University of Mons (Belgium), 1983.

[12] S. Trainoff, G. Ahlers, and D. S. Cannel (private communication).

[13] M. T. Ouazzani, J. K. Platten, H. W. Müller, and M. Lücke, Int. J. Heat Mass Transfer. (to be published).

[14] H. W. Müller, M. Lücke, and M. Kamps, Europhys. Lett. **10**, 451 (1989); Phys. Rev. A **45**, 3714 (1992).

[15] For a review, see P. Heurre, in *Instabilities and Nonequilibrium Structures*, edited by E. Tirapegui and D. Villarroel (Reidel, Dordrecht, 1987), p. 141.

[16] M. T. Ouazzani, J. K. Platten, and A. Mojtabi, Int. J. Heat Mass Transfer **33**, 1417 (1990).

[17] H. R. Brand, R. J. Deissler, and G. Ahlers, Phys. Rev. A **43**, 4262 (1991).

[18] H. W. Müller, M. Tveitereid, and S. Trainoff, Phys. Rev. E **48**, 263 (1993).

[19] K. S. Gage and W. H. Reid, J. Fluid Mech. **33**, 21 (1968).

[20] J. K. Platten and J. C. Legros, *Convection in Liquids* (Springer, Berlin, 1984).

[21] H. B. Squire, Proc. R. Soc. London Ser. A **142**, 621 (1933).

[22] R. Tagg, W. S. Edwards, and H. L. Swinney, Phys. Rev. **42**, 831 (1990).

[23] R. J. Deissler, J. Stat. Phys. **40**, 371 (1985).

[24] R. D. Deissler, Physica D **25**, 233 (1987).

[25] R. J. Deissler, J. Stat. Phys. **54**, 1459 (1989).

[26] K. L. Babcock, G. Ahlers, and D. S. Cannell, Phys. Rev. Lett. **67**, 3388 (1991).

[27] K. L. Babcock, D. S. Cannell, and G. Ahlers, Physica D **61**, 40 (1992).

[28] A. Tsameret and V. Steinberg, Phys. Rev. Lett. **67**, 3392 (1991).

[29] G. J. Hwang and C. L. Liu, Can. J. Chem. Eng. **54**, 521 (1976).

[30] G. J. Hwang and K. C. Cheng, J. Heat Transfer **95**, 72 (1973).